This is the Pre-Published Version.
This is the peer reviewed version of the following article: Chen, S., Tao, X., Zeng, W., Yang, B., & Shang, S. (2017). Quantifying energy harvested from contact-mode hybrid nanogenerators with cascaded piezoelectric and triboelectric units. Advanced Energy Materials, 7(5), 1601569, which has been published in final form at https://doi.org/10.1002/aenm.201601569. This article may be used for non-commercial purposes in accordance with Wiley Terms and Conditions for Use of Self-Archived Versions. This article may not be enhanced, enriched or otherwise transformed into a derivative work, without express permission from Wiley or by statutory rights under applicable legislation. Copyright notices must not be removed, obscured or modified. The article must be linked to Wiley's version of record on Wiley Online Library and any embedding, framing or otherwise making available the article or pages thereof by third parties from platforms, services and websites other than Wiley Online Library must be prohibited.

Quantifying Energy Harvested from Contact-Mode Hybrid Nanogenerators with Cascaded Piezoelectric and Triboelectric Units

Song Chen, Xiaoming Tao, Wei Zeng, Bao Yang, Songmin Shang*

Nanotechnology Center of Functional and Intelligent Textiles and Apparel

Institute of Textiles and Clothing, The Hong Kong Polytechnic University, Hong Kong

E-mail: xiao-ming.tao@polyu.edu.hk

Abstract

This paper presents an investigation of novel contact-mode hybrid nanogenerators comprising cascaded piezoelectric and triboelectric units. For the first time, a theoretical analysis of the contact-mode hybrid generator is presented to describe the relationships among transfer charges, voltage, current and average output power in terms of materials properties, hybrid generator structural parameters, harvesting and operational conditions. New hybrid generators with much enhanced piezoelectricity are fabricated via a simple, room-temperature, cost-effective route by using nonwoven fabrics made from electrospun Polyvinyledenedifluoride-trifluoroethylene (PVDF-TrFE)/Ag nanowire nanofibers and Polydimethylsiloxane (PDMS) composites with graphite nanoparticles. The results provide a powerful tool for synthesis and selection of materials, design and optimization of the configuration and operation of such kind of hybrid generators as well as determination of the value of external capacitor.

Keywords: Energy harvesting, Hybrid generator, Piezoelectric generator, Triboelectric generator, Piezoelectric polymeric nanocomposite

1. Introduction

In the last decades, due to the advancements in circuitry efficiency and miniaturization, much lower power consumption of micro-electronic devices has been achieved. As a result, rechargeable batteries with high energy storage have been widely used in portable and wearable electronics. Meanwhile, renewable, affordable and green energy has shown noticeable advantages for them and has driven numerous research efforts both in industries and academia.[1-3] Energy harvesting technologies from sources such as solar, thermal and mechanical energy (vibration, human motion, air flow, etc.) have been increasingly explored as alternative and sustainable routes of energy supply.[2,4-9] Among them, mechanical energy is significant and relatively stable.

Various methods have been investigated such as piezoelectric, triboelectric and electromagnetic energy harvesting technologies. Piezoelectric nanogenerators made from zinc oxide (ZnO),[10] gallium nitride (GaN),[11,12] lead zirconate titanate (PZT),[13,14] barium titanate ($BaTiO_3$),[15,16] piezoelectric polymeric (PVDF) and piezoelectric composites (for example PDMS with piezoelectric ceramic nanomaterials) have been reported. Addition of conductive or semi-conductive fillers, such as carbon nanotube[17], carbon nanofiber (CNF),[18] graphite nanoplates,[19] Ag nanoparticules[20] have led to enhanced electric power output because of the increased dielectric constant with low dielectric loss in polymeric composite materials. On the other hand, due to its high

open-circuit voltage, triboelectricity has been studied to harvest mechanical energy in contact mode or sliding mode, based on the contact induced electrification[9] when two materials get in contact or rub against each other.[21] PTFE and PDMS with high triboelectric affinity values thus have been used for making triboelectric generators.[22] Prototypes of triboelectric generators and self-powered systems with variations in structures and surface patterns have been reported, for instance, r-shape,[22] rotating disk,[23] nano or micrograting surface,[24] and single or double electrodes.[25]

Hybrid generators (HG) with piezoelectric and triboelectric units have advantages when working in contact mode[26] as they are preferred for applications such as large-area of floor coverings like run-ways and carpets, as well as foot-mounted wearable electronic systems,[27,28] because a short vertical displacement is involved and easy in integration. However, their working mechanism remains elusive although some authors believed that the enhanced piezoelectricity exits due to such hybridization.[22] Most published papers are experimental investigations only. Up to now, there has been no theoretical treatment of the charge generation and transfer processes as well as power output of such HGs. The fundamental understanding of the mechanisms and, in particular, a theoretical model would be very useful for the design, fabrication and optimization of the HGs.

In this paper, contact-mode HGs were designed and fabricated by using PVDF-TrFE/Ag nanowires (PTAN) nanofiber fabric as the piezoelectric layer, a

PDMS/graphite composite as the triboelectric layer and three fabric electrodes in a cascaded structure. The piezoelectric layer was made by a novel, simple, low-cost, and effective method. Ag nanowires were used to enhance piezoelectricity, electric conductivity of PVDF-TrFE nanofibers, and to achieve a high dielectric constant and low dielectric loss. Graphite nanoparticles were utilized to increase the dielectric constant of triboelectric layer which had no additional surface micro-/nano modification. The working mechanism was proposed, based upon which, a theoretical treatment of the tandem triboelectric and piezoelectric HG in contact mode with loads of either resistance or capacitance has been developed, for the first time.

2. Results and Discussion

2.1. Structure of Fabricated HG

As shown in Figure 1a,b, in the fabricated HG, the piezoelectric unit and triboelectric unit are arranged in a cascaded fashion. The sandwich structure comprises five layers: top fabric electrode, PDMS/graphite nanocomposite film as the triboelectric material, middle fabric electrode, PTAN nanofiber layer as the piezoelectric materials, and the fabric electrode on the bottom. The triboelectric unit has the two electrodes and the PDMS composite dielectric layer. The piezoelectric unit consists of the two fabric electrodes and nanofiber layer. The middle fabric electrode played dual roles as: an electrode of piezoelectric unit and the contact surface of triboelectric unit. The thickness of the piezoelectric layer and triboelectric layer was about 200 and 370 μm, respectively. Poly (methyl methacrylate) (PMMA) plate was selected as the covers for

its suitable rigidity, easy fabrication and low cost. Four springs were utilized to connect the two cover plates at the corners with a narrow space between them. The rough surface of fabric electrode is shown in Figure 1c.

Figure 1d shows the Ag nanowires with the diameter of ≈120 nm and length of 25~40 μm by scanning electron microscopy (SEM) images. The diameter of as-spun randomly oriented PTs nanofibers ranges from 200 to 700 nm (Figure 1e). In Figure 1f,g, Fourier transform infrared spectroscopy (FTIR) and X-ray diffraction (XRD) are utilized to evaluate the crystalline quality of the PTAN nanofiber. FTIR spectrum of the as-spun nanofibers exhibits strong vibration peaks at 840 and 1280 cm^{-1}, which indicates the formation of β crystalline phase.[23] XRD data measured indicate a strong β phase crystalline signal with 2θ at 20°, as shown in Figure 1g. Due to the increase of Ag nanowires, β crystalline phase was enhanced and the crystallinity increased from 67% to 92%, which means higher piezoelectric properties. This β-phase increase can be attributed to interactions between the Ag nanowires and the PVDF-TrFE matrix, which forces the polymer chains to be embedded into the β phase crystalline. Since Ag nanowires have an electron-rich surface, C-F bonds on the PVDF-TrFE chain are electron-deficient groups. And the interactions between Ag nanowires and PVDF-TrFE, which force the polymer chain to expand in a TTT conformation and overlie on the surface of Ag nanowires. This local trans conformation may facilitate the nucleation of a polar β phase, which was confirmed in other work.[29, 30] Therefore, the formation of high β phase in the as-synthesized nanofibers allows us to utilize it to fabricate

piezoelectric units and hybrid generators. Figure 1h demonstrates the SEM images of cross-section of a typical PDMS composite film with 3 wt% proportion of graphite nanoparticles and the thickness of the film is about 370 μm. The proportions of Ag nanowires and graphite nanoparticles were optimized according to the power output of the individual units.

2.2.Performance Characteristics of HG

The effects of graphite nanoparticles in the PDMS composites on the harvested power were examined in detail by using the HG samples of size (6 cm × 6 cm ×370 μm). Since the triboelectric and piezoelectric units are not working in phase, a double-bridge rectifier circuit was used with a connected capacitor of 100 V/100 μF (Figure 2), which was charged 1220 times with a maximum force of 1500 N and 3 Hz by HG. Optimization of material components was conducted and results are given in the supplementary information. As shown by Figures S1 and S2 (Supporting Information), the best materials are the PDMS composite with 3.0 wt% graphite nanoparticles and PVDF-TrFE nanofiber nonwoven fabric with 2.0 wt% Ag nanowires, yielding the highest average output power. Hence, they have been selected to make a HG for full characterization. The optimized HG has charged the capacitor to 11.57 V after 1220 compression cycles at 3 Hz and generated a total time-averaged power of 16.46 μW.

A typical HG shows a measured peak voltage output of 247.87 V by its piezoelectric unit (Figure 3a) and a voltage output of 84.43 V (Figure 3b) by its triboelectric unit,

respectively. Under an external resistance of 5.1MΩ, the HG exhibits the peak measured current of 31.63 μA from its piezoelectric unit (Figure 3c) and of 10.65 μA from its triboelectric unit (Figure 3d), respectively. The voltage output transforms between zero and a plateau value, respectively, which corresponds to the movement of contact surfaces. As demonstrated in Figure 3e,f, the momentary current drops by increasing load resistance are caused by Ohmic loss, while the voltage is enhanced. The instantaneous power output ($W = I_{peak}^2 \times R$) reached its maximum at a resistance load of 2.4 MΩ.

Moreover, the power output of the HG combined piezoelectric output and triboelectric output in parallel, but the polarity and phase of the piezoelectric and triboelectric output are not synchronous, which would degrade the total output performance of the HG. Consequently, a full-wave bridge rectifier circuit was utilized to rectify the voltage outputs of HG and two bridges were independently connected to the piezoelectric and triboelectric units.

Figure 4a-c demonstrates the rectified open-circuit voltages of the piezoelectric unit, triboelectric unit and HG under the cyclic compression force. The rectified current output of HG with 5.1 MΩ and 2.5 MΩ resistance load is 38.16 μA and 40.09 μA, respectively, as shown in Figure 4d,e. The HG in parallel connection charged a 100 V/100 μF capacitor. After 1220 cycles, the voltage of the capacitor reached 11.57 V and the average power output was 16.46 μW, which is larger than the sum of the

piezoelectric power and triboelectric power by charging two capacitors separately. This may be caused by the reduction of internal resistance attributed to the parallel connection. According to the calculation and experimental results, 2.5 MΩ is the optimal impedance with the highest peak power output, about 6.25 mW. The results also demonstrate that the power output should be connected in parallel after being rectified by two full-wave bridge rectifier circuit to avoid the cancellation of the piezoelectric and triboelectric power. Moreover, the power output was used to light up a LED pattern consisting of 53 LEDs as shown in Figure 4f.

2.3.Working Mechanism

The working mechanism of HG is proposed, in Figure 5, by combining the piezoelectric, triboelectric and electrostatic effects. There are two units of the HG: the piezoelectric unit comprising a piezoelectric active layer and two electrodes, and the triboelectric unit with a triboelectric layer and electrodes. The piezoelectric unit has two roles: piezoelectric generator and triboelectric surface.

The moving plate of the keyboard life tester moves up and down with a separation distance, *g*, from the electrode 1. If this separation distance becomes zero, the electrode 1 fully follows the motion of the moving plate. Another separation distance between the dielectric layer and electrode 2 is defined as *x,* shown in Figure 5a. The total displacement of the dielectric layer and the piezoelectric layer is defined as η. One

period motions of the moving plate can be divided into five stages: Δt_1 (from t_1 to t_2, the moving palate moves up from $\eta = \eta_{max}$ to $\eta = 0$, piezoelectric generator are active and the force expresses a fast decrease), Δt_2 (from t_2 to t_3, the moving palate moves up from $x = 0$ to $x = x_{max}$ and $\eta = 0$. The triboelectric generator is active), Δt_3 (from t_3 to t_4, the moving palate moves up and down between $g = 0$ and $g = g_{max}$, both generators are inactive), Δt_4 (from t_4 to t_5, the moving palate moves down from $x = x_{max}$ to $x = 0$, the triboelectric generators are active), and Δt_5 (from t_5 to t_6, the moving palate moves down from $\eta = 0$ and $\eta = \eta_{max}$, the piezoelectric generator is active and the force has a fast increase), as shown in Figure 5b. After contacted with each other, the contact surface of the dielectric layer and electrode 2 has opposite triboelectric charges of an equal areal density due to contact electrification. After sufficient contact, the surface charges of electrode 2 and the dielectric layer both reach a saturation state. It is reasonable to assume that the tribo-charges are uniformly distributed on the dielectric layer with negligible decay (denoted as surface charge density, σ, as shown in Figure 5c).

During the stage of Δt_1, when moving plate moves up with decrease of η from $\eta = \eta_{max}$ to $\eta = 0$ and an external force begins to release. As soon as the external mechanical force is released, compression stress of the piezoelectric unit is reduced to zero (at the moment of t_2), piezoelectric potentials are generated and reverse piezoelectric output appears with the external connection, as shown in Figure 5d. During the stage of Δt_2 in Figure 5e, the contact surfaces begin to separate because of the restoring force in the springs and the gap distance x increases to x_{max}, resulting in the change of electric field

in accordance with the theory of electrical field in capacitance. Electrons are driven back from the electrode 2 to electrode 1 via external circuit. After reaching the charge equilibrium, current begins to decrease to zero (falling edge). The middle fabric electrode plays dual roles of the contact surface and electrode in the HG. The charge transfer rate determines the triboelectric current output hence the performance of HG. In the period of Δt_3, moving plate moves up and down without electrical output generated.

During Δt_4, the gap of x begins to decrease from x_{max} to 0 and electrons are driven from electrode 1 to electrode 2 with reverse triboelectric output with external connection as demonstrated in Figure 5f. The reduction of the gap distance increases the charge transfer while the generated voltages decrease the charge transfer until reaching a charge equilibrium. After that, the generated current begins to decrease, leading to the falling edge of voltage and current output. At the moment of t_5, PDMS surface contacts with electrode 2 and the current generated by charge transfers decline to zero.

During the stage of Δt_5, the piezoelectric charges are generated due to the compression stress, as shown in Figure 5c. The piezoelectric potential will generate forward piezoelectric output between electrode 2 and electrode 3 of the piezoelectric unit. In consequence, the HG achieves a compression cycle. The enlarged inset curves in Figures 3a,b illustrate the characteristics of open-circuit voltage of the piezoelectric unit and triboelectric unit in one cycle, which validate the working mechanism.

2.4. Theoretical analysis of HG

Figure 6 illustrates the proposed working scheme for analysis. The dielectric layer with thickness of d_1 and relative dielectric constant of ε_r is the dielectric part of triboelectric generators. If one assumes that the tribo-charges are evenly distributed on the triboelectric layer surface with a small decay, the area is much larger than the separation distance and only vertical components of the electric fields exist in the air gap, triboelectric and piezoelectric layers, the following treatment can be applied. The distance (x) between the two top electrode and triboelectric layers will be varied under an external mechanical force. Within the triboelectric unit, the two layers have opposite charges (triboelectric charge) with the average density of σ in their contact area S. After separating of the two layers, $x(t)$ would increase and the surface charge density of electrodes are changed due to electrostatic induction and the surface charge density of electrodes are denoted as σ_1, σ_2, and σ_3, respectively, which satisfy the following conservation condition:

(1)

The voltage of the close loop with external circuits shown in Figure 5i should stratify the following condition:

$$\sum_{i=1}^{N} V_i = 0 \qquad (2)$$

where V_i represents the voltage of the i^{th} part in the close loop.

Since both the length and width of the dielectric layer and electrodes are several orders of magnitude larger than its effective separation distance x, the thickness d_1 of dielectric and the thickness d_2 of piezoelectric, respectively, the corresponding electric fields can be simply calculated by Gauss's law, the electric field strength at each area inside the device can be expressed as:

In the piezoelectric unit: (3)

In the air gap: (4)

In the triboelectric unit: (5)

According to equation (2), one can obtain

(6)

(7)

In this case at $t = 0$ (i.e., t_1 as shown in Figure 5b), the two contacting layers are close to each other for a sufficiently long time so that the contact electrification reaches its saturation as shown in Figure 5c. The amount of the charges on electrode 1, electrode 2 and electrode 3 are defined as Q_1, Q_2, and Q_3, respectively. Initial conditions are given by

(8)

(9)

(10)

where $\boldsymbol{S}$ is the areal size of dielectric layer.

The surface density on electrodes is calculated by

(11)

(12)

(13)

According to the Ohm's law, the output voltages are expressed as

(14)

(15)

Merging equations (3) - (6), (7), (14), and (15), one can have

(16)

(17)

By combining the initial conditions in equation (10), differential equation (14) is solved analytically in a way similar to our previous verified model for contact-mode triboelectric generato[7]

(18)

(19)

The separation distance, x, between the dielectric layer and electrode 2 is expressed as

(20)

where θ_1 and θ_2 are determined by the max separation distance, g, between the moving plate and the top electrode.

From Equations (18) and (19), the current is given by

(21)

(22)

According to the analysis of HG, in the period of $\Delta t_2, \Delta t_4$, there is only triboelectric output between electrode 1 and electrode 2, resulting in transfer charge. If

$R_1 \frac{S}{\frac{x(t)}{\varepsilon_0}+\frac{d_1}{\varepsilon_{r1}}} << \Delta t_2 = \Delta t_4$, it is reasonable to assume that the charges on electrode 1 have fully gone back to electrode 2 when the triboelectric surfaces fully contact with each other.

Then the moving plate moves down and up during Δt_5 and Δt_1, the piezoelectric unit is under compression. There is only piezoelectric output caused by compression stress

(23)

where V is the voltage between top and bottom electrode; d_{31} and d_{33} are the piezoelectric constant in the vertical and horizontal direction of the film, respectively, Y_c is the thickness, w and l are the width and length respectively, s_1 and s_3 are the corresponding strain components. The voltages in periods Δt_5 and Δt_1 are

(24)

The generated output should be rectified via the rectifier bridge circuit as shown in Figure 2, making it possible to charge a capacitor and battery or to supply power to wearable or portable electronics. In this analysis, an external capacitor is used.

When the capacitor is charged for *n* times, the total storage charge of the capacitor, *Q(t),* is given by

(25)

where

(26)

(27)

The average power P in a period t can be obtained from the following equations

$$\begin{aligned} Q &= C \times U \\ P &= \frac{1}{2} \times C \times U^2 / t \end{aligned} \qquad (28)$$

According to this analysis, the amount of transfer charge decreases when the number of charge cycles increases. It also can be employed to optimize value of external capacitor according to the theory of extract circuit.

3. Conclusion

In this work, by using PTAN nanofibers and PDMS/graphite nanocomposites as the active layers, the effects of piezoelectricity and triboelectricity are combined into a single HG. The inclusion of Ag nanowires promoted the formation of the β-phase

crystals and enhanced piezoelectricity of the PTAN nanofibers. With a 3 Hz cyclic compression force, the peak voltage and average power output of the HG reached 190 V and 16.46 μW, respectively. Furthermore, this new approach is effective to significantly improve power output of the constitutive units as well as the HG by using conductive fillers in the composites for piezoelectric layer or dielectric layer with increased respective dielectric constants and low dielectric loss. The fabrication process is a simple, room-temperature, low-cost, and effective one. Superposition of the piezoelectric and triboelectric outputs is evident at all five separate working stages during one compression cycle.

For the first time, a theoretical analysis of the contact-mode hybrid generator has been developed to describe the relationships among transfer charges, voltage, current, and average output power in terms of materials parameters, HG structural parameters, harvesting, and operational conditions. The theoretical analysis would provide a powerful tool for material synthesis and selection, design, and optimization of the configuration and operation of hybrid generators as well as the value of external capacitor. The noticeably high power output of the HG can be used as a power source in wearable electronics to extend the life of battery.

4. Experimental Section

Fabrication of PTAN Nanofibers

PVDF-TrFE (70/30) powder (Department of Applied Physics, the Hong Kong Polytechnic University) were thoroughly dissolved in the mixture of N, N′-dimethylformamide and acetone (mass ratio, 4:1) at 80 ℃ to prepare the PVDF-TrFE electrospun solution (18%, w/w). Then the Ag nanowires (Nanjing XFNANO Materials TECH Co., Ltd, 120 nm diameter and 20 μm average length) were simultaneously added to the mixture with the mass ratio from 0:100 to 3:97. The mixture was stirred for 4 hours and sonicated for another 1 h to reach sufficient homogeneity. The homogeneous solution was then placed into a 20 ml plastic syringe with a stainless steel nozzle of 1 mm in diameter for electrospinning. The rotating collector was covered by a piece of conductive fabric electrode. The power was supplied via the stainless steel nozzle. The voltage was 32 kV with 28 kV positive voltage and 4 kV negative voltage, and the tip-to-collector distance was 10 cm.

Fabrication of PDMS/Graphite Nanocomposite Films

Monomers for PDMS and cross-linking agent (XE15-645, Momentive) were mixed with a mass ratio of 1:1 to prepare PDMS solution. Then graphite particles with an average diameter of 30 nm (Nanjing XFNANO Materials TECH Co., Ltd, 30 nm diameter) were added into the PDMS solution and were thoroughly dispersed with petroleum ether via magnetic stirrer for 3 h. After the graphite particles were dispersed, the solution was transferred to the fabric electrode fixed on a glass mold prepared as substrate with the area size of 6 cm × 6 cm. After vacuumed, the mold was placed into an oven at 80 ℃ for 4 h. When the PDMS/graphite composite film was formed and

solidified, the thickness of the film was about 280 μm. The mass ratio of graphite particles was from 0% to 5%. Finally, the fabricated composite film was assembled to form the HG.

Characterization

Scanning electronic micrographs (SEM) for the samples were taken by a field emission scanning electron microscope (SEM, JEOL JSM-6335F) at an accelerating voltage of 200 kV. X-ray diffraction patterns were obtained by D/MAX-IIIC X-ray diffractometer (Rigaku, Tokyo, Japan). Fourier transform infrared (FTIR) spectrum was measured by FT-IR spectrometer (Spectrum 100, PerkinElmer, US.).

Measurement System

The output performance of piezoelectric and hybrid generators were evaluated by utilizing a lab-made cyclic compression system with frequency ranging from 0 to 5 Hz. The compression system was consisted of a DC motor, force sensor and accessories to achieve cyclic compression movement. The force signal was monitored by DAQ unit (Dewetron, Dewe-2600 DAQ system) and the peak value was set at 1500 N. When the fabricated HG (6 cm × 6 cm) was compressed by the cyclic compression system at 3 Hz, the voltages and current with resistance load of piezoelectric unit and triboelectric unit of HG were measured separately by Keisight DSO-X3014A oscilloscope with 1 MΩ internal resistance and N2790A high voltage probe (maximum 1400 V) with 8 MΩ internal resistance. The resolution was 8 digits and the precision was 2.26% full scale.

In addition, for the average power, the rectifier circuit described in Figure 6 was employed and a capacitor of 100 μF/100 V was used as load. There were three specimen used for each sample and each specimen was tested three times. After 1220 times compression, the average voltages of capacitor were measured using DSO-X3014A to calculate the power.

Supporting Information

Supporting Information is available from the Wiley Online Library or from the author.

Acknowledgements

The authors acknowledge the partial funding support from the Research Grants Council of Hong Kong SAR Government (Project Nos. PolyU5272/11E, PolyU5251/13E and PolyU152152/14E). S.C. thanks The Hong Kong Polytechnic University for a postgraduate scholarship.

References

[1] J. A. Paradiso and T. Starner, *IEEE Pervasive Comput*. 2005, 4, 18.

[2] X.M. Tao, Handbook of Smart Textiles, 2015, Springer, Germany 2015.

[3] V. S. Arunachalam, E. L. Fleischer, *MRS Bull*, 2008, 33, 264.

[4] Y. Qi, and M. C. McAlpine, *Energy Environ. Sci*, 2010, 3, 1275.

[5] W. Zeng W, L. Shu, Q. Li, S. Chen, F. Wang and X. M. Tao, *Adv Mater* 2014, 26(31):5310.

[6] H. D. Espinosa, R. A. Bernal and M. M. Jolandan, *Adv. Mater*, 2012, 24, 4656.

[7] B. Yang, W. Zeng, Z. H. Peng, S.R. Liu and X.M. Tao, *Adv. Energy Mater*, 2016, 6,1600505.

[8] Z. L. Wang, G. Zhu, Y. Yang, S. Wang and C. Pan, *Mater. Today,* 2012, 15, 532.

[9] Z. L. Wang, *ACS Nano*, 2013, 7, 9533.

[10] Z. L. Wang and J. H. Song, *Science,* 2006, 312, 242.

[11] L. Lin, C. H. Lai, Y. Hu, Y. Zhang, X. Wang, C. Xu, R. L. Snyder, L. J. Chen, Z. L. Wang, *Nanotechnology*, 2011, 22, 475401.

[12] C. Y. Chen, G. Zhu, Y. F. Hu, J. W. Yu, J. H. Song, K. Y. Cheng, L. H. Peng, L. J. Chou, and Z. L. Wang, *ACS Nano*, 2012, 6, 5687.

[13] X. Chen, S. Xu, N. Yao and Y. Shi*, Nano Lett*, 2010, 10, 2133.

[14] C. Y. Chen, T. H. Liu, Y. Zhou, Y. Zhang, Y. L. Chueh, Y. H. Chu, J. H. He and Z. L. Wang, *Nano Energy*, 2012, 1, 424.

[15] K. I. Park, S. Xu, Y. Liu, G. T. Hwang, S. J. Kang, Z. L. Wang, K. J. Lee, *Nano Lett*, 2010, 10 (12), 4939.

[16] Z. H. Lin, Y. Yang, J. M. Wu, Y. Liu, F. Zhang and Z. L. Wang, *J. Phys. Chem. Lett*, 2012, 3, 3599.

[17] C. Yang, Y. H. Lin, C.W. Nan, *Carbon*, 2009, 47(4), 1096.

[18] L. L. Sun, B. Li, Y. Zhao, G. Mitchell and W. H. Zhong, *Nanotech*, 2010, 21, 305702.

[19] F. He, S. T. Lau, H. L. Chan, J. T. Fan, *Adv Mater*, 2009, 21(6), 710.

[20] W. Zheng, X. F. Lu, W. Wang, Z. J. Wang, M. X. Song, Y. Wang, C. Wang, Phys. Status Solidi A: Appl. *Mater Sci*, 2010, 207, 1870.

[21] P. E. Shaw, *Proc. R. Soc. A* 1917, 94, 16.

[22] M. D. Han, X. S. Zhang, B. Meng, W. Liu, W. Tang, X. M. Sun, W. Wang, and H. X. Zhang,

ACS Nano, 2013, 7, 8554.

[23] C. Zhang, T. Zhou, W. Tang, C. B. Han, L. M. Zhang, and Z. L. Wang. *Adv Energy Mater.* 2014, 4, 1301798.

[24] G. Zhu, Y. S. Zhou, P. Bai, X. S. Meng, Q. S. Jing, J. Chen, and Z. L. Wang. *Adv Mater*, 2014, 26, 3788.

[25] Y. Yang, Y. S. Zhou, H.L. Zhang, Y. Liu, S. M. Lee, and Z. L. Wang. *Adv Mater*, 2013, 25, 6594.

[26] W. Zeng, X. M. Tao, S. Chen, S. Shang, H. L. W. Chan and S. H. Choy, *Energy Environ Sci*, 2013, 6, 2631.

[27] L. Shu, T. Hua, Y. Y. Wang, Q. A. Li, D. D. Feng and X. M. Tao, *IEEE. Trans. Inf. Technol. Biomed*. **2010**, *14*, 767.

[28] L. Shu, X. M. Tao, D. D. Feng, *IEEE Sens. J*. **2015**, *15*, 442.

[29] D. Mandal, K. J. Kim, J. S. Lee, *Langmuir*, 2012, **28**, 10310.

[30] B. Z. Li, C. Y. Xu, J. M. Zheng, C. Y. Xu, *Sensors-Basel*, 2014, 14, 9889-9889.

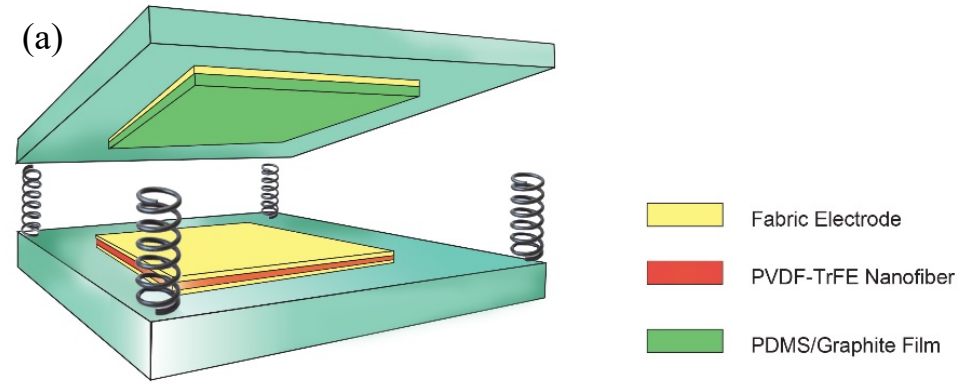
(a)
Fabric Electrode
PVDF-TrFE Nanofiber
PDMS/Graphite Film

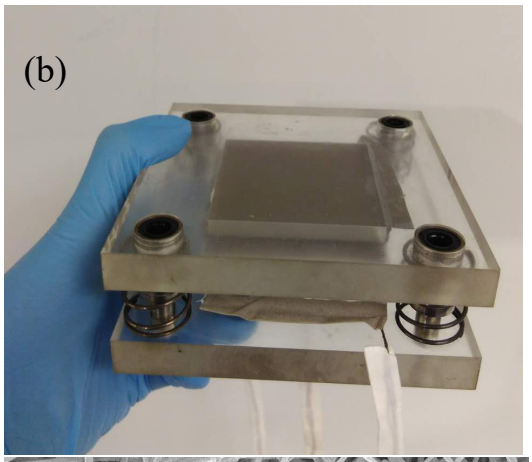
(b)

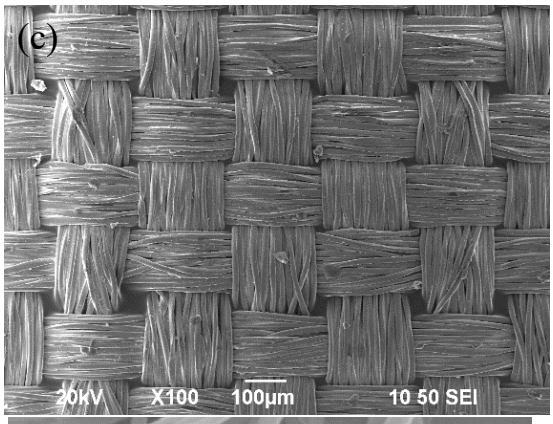
(c)
20kV X100 100µm 10 50 SEI

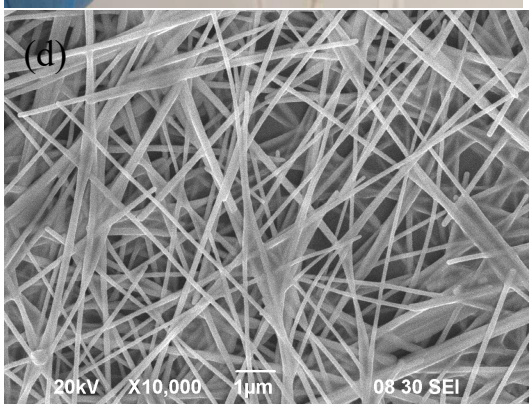
(d)
20kV X10,000 1µm 08 30 SEI

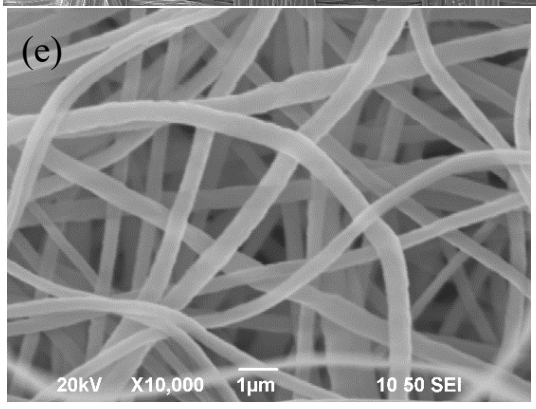
(e)
20kV X10,000 1µm 10 50 SEI

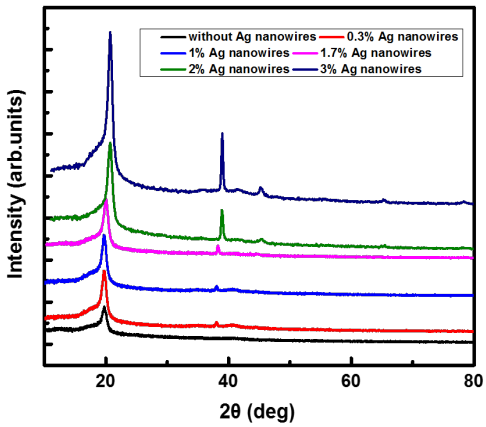
without Ag nanowires
0.3% Ag nanowires
1% Ag nanowires
1.7% Ag nanowires
2% Ag nanowires
3% Ag nanowires
Intensity (arb.units)
20
40
60
80
2θ (deg)

(f)

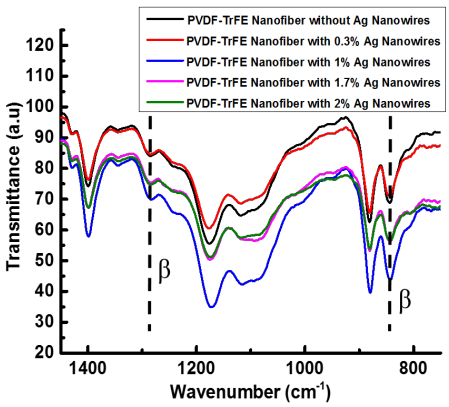
PVDF-TrFE Nanofiber without Ag Nanowires
PVDF-TrFE Nanofiber with 0.3% Ag Nanowires
PVDF-TrFE Nanofiber with 1% Ag Nanowires
PVDF-TrFE Nanofiber with 1.7% Ag Nanowires
PVDF-TrFE Nanofiber with 2% Ag Nanowires
Transmittance (a.u)
120
110
100
90
80
70
60
50
40
30
20
β
β
1400
1200
1000
800
Wavenumber (cm-1)

g)

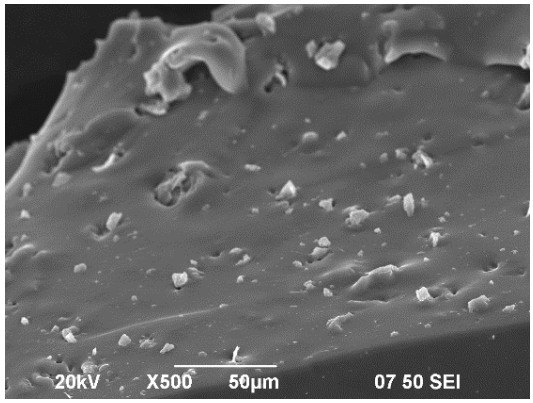

(h)

Figure 1. a) Schematic diagram of HG. b) Photograph of HG. c) Scanning electron microscopy (SEM) image of conductive fabric electrode. d) SEM image of Ag nanowires. e) SEM image of PTs nanofibers with 2% Ag nanowires. f) Fourier transform infrared spectroscopy (FTIR) of PVDF-TrFE/Ag nanofiber. g) X-ray diffraction of PVDF-TrFE/Ag nonwoven fabric indicating the formation of the beta-phase. h) SEM images of PDMS composite film with 3 wt% graphite nanoparticles.

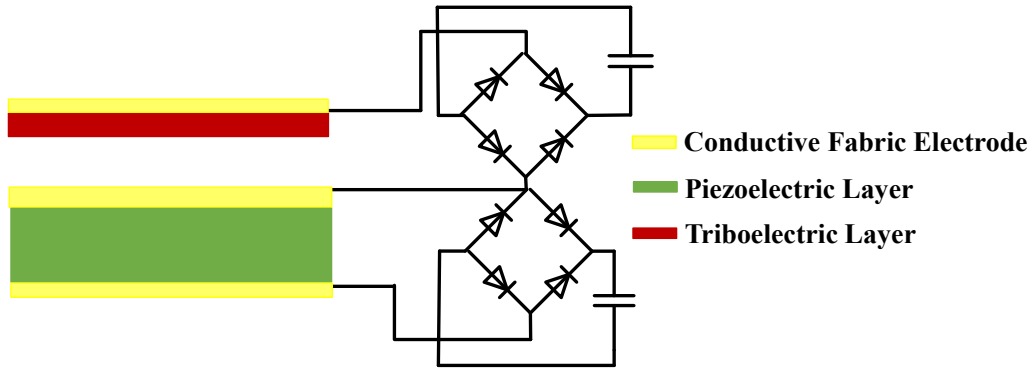

(a)

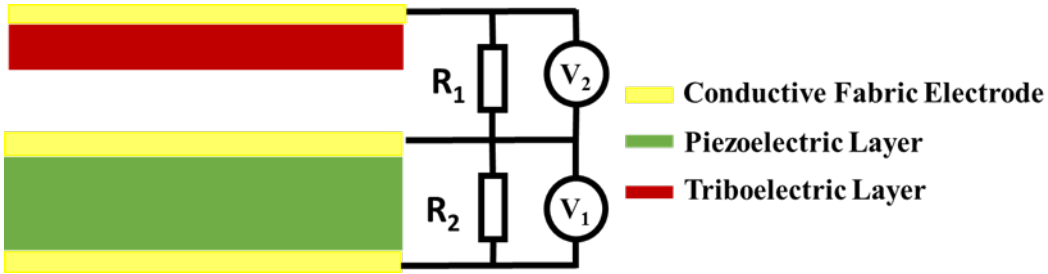

(b)

Figure 2. Equivalent measurement circuit of the HG: a) charge two capacitors and b) with two resistance load.

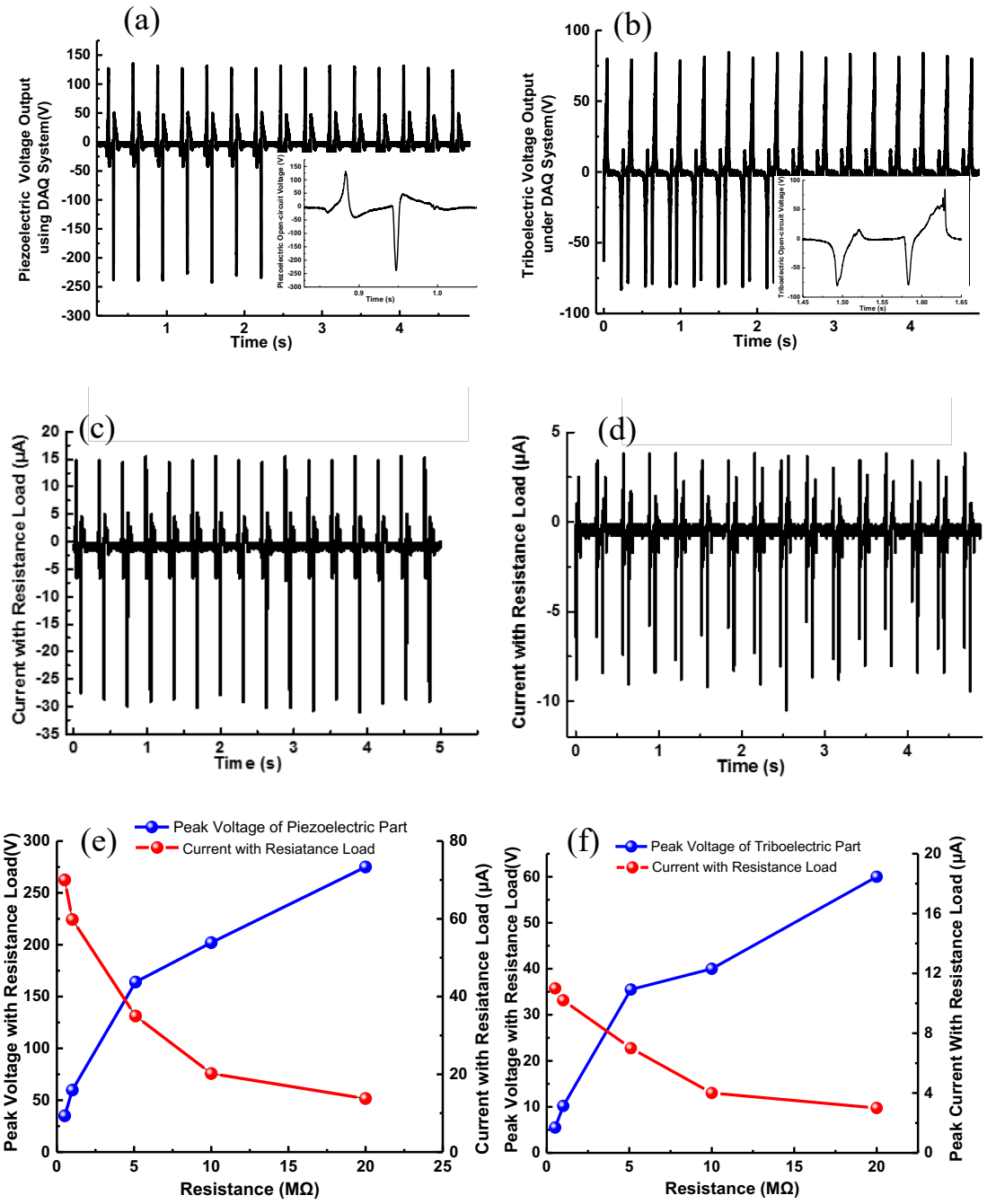

Figure 3. Output characteristics of optimized HG with a peak compression force of 1500 N and frequency of 3Hz. a) Voltage output of the piezoelectric unit. Inset shows an enlarged voltage curve in one cycle. b) Voltage output of the triboelectric unit. Inset shows an enlarged voltage curve in one cycle. c) Current output of the piezoelectric unit with 5.1 MΩ external resistance. d) Current output of the triboelectric unit with 5.1 MΩ external resistance. e) Peak voltage and current output of the piezoelectric unit versus the external resistance. Increasing load resistance yields a higher peak voltage output but lower peak current output. f) Peak voltage and current output of the triboelectric unit versus external resistance. Increasing the external resistance gives a higher peak voltage output but lower peak current output.

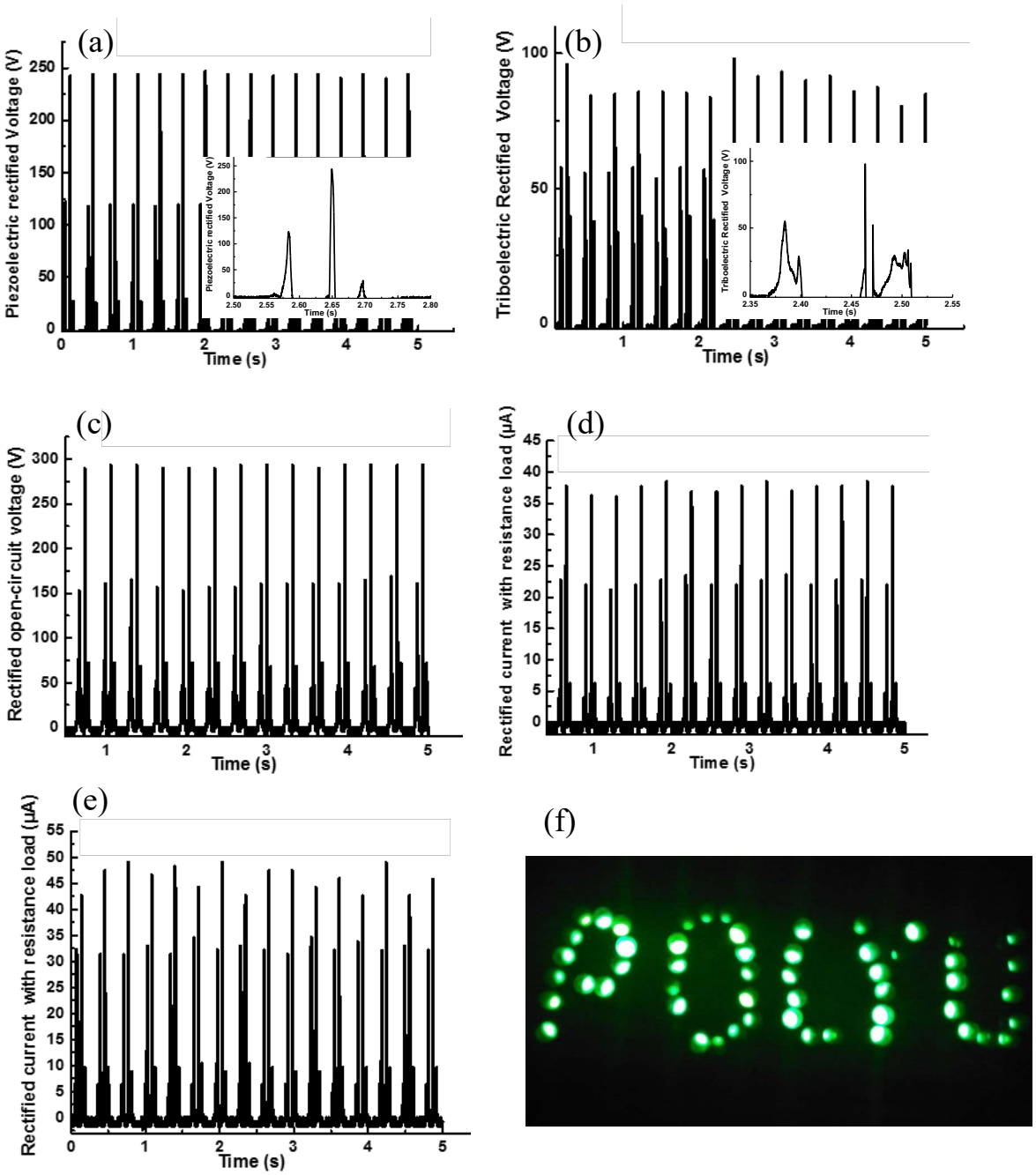

Figure 4. Rectified voltage output a) of the piezoelectric unit, b) of the triboelectric unit, c) of HG in parallel connection. d) Rectified current output of HG in parallel connection with 5.1 MΩ external resistance. e) Rectified current output of HG in parallel connection with 2.5 MΩ resistance load. f) LED arrays powered by the HG.

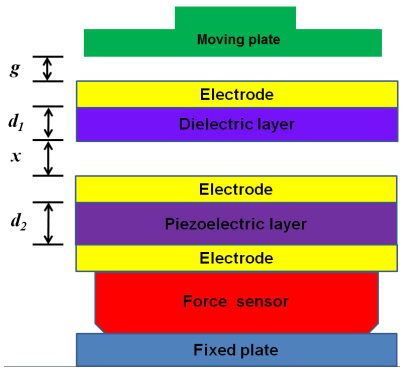

(a)

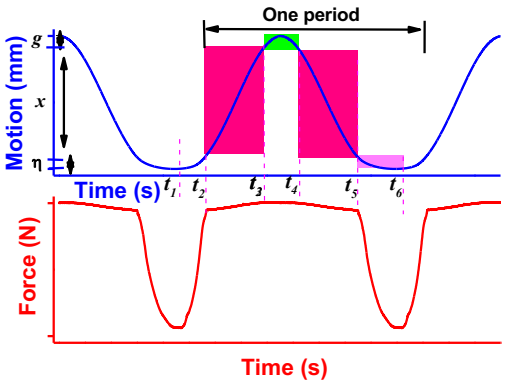

(b)

(c) t=0

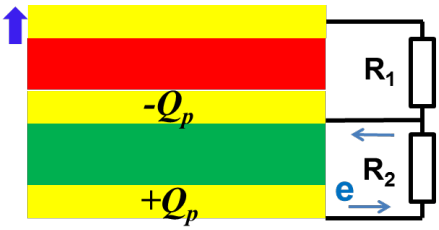

(d) Δt_1

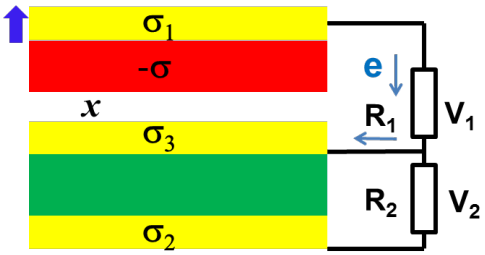

(e) Δt_2

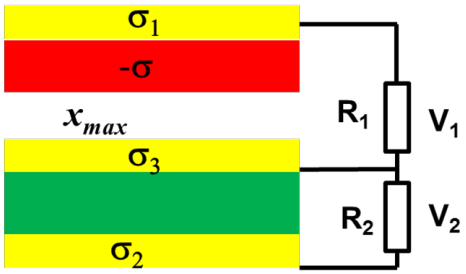

(f) $t=t_3$

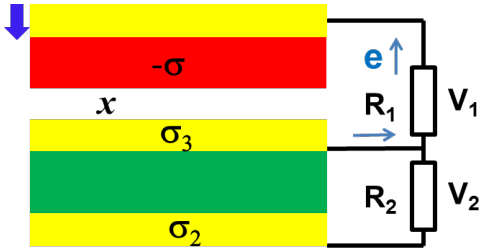

(g) Δt_4

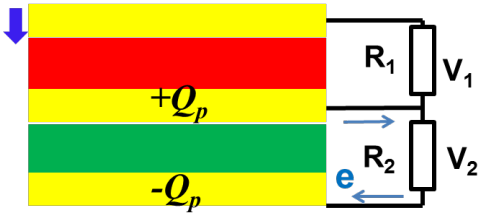

(h) Δt_5

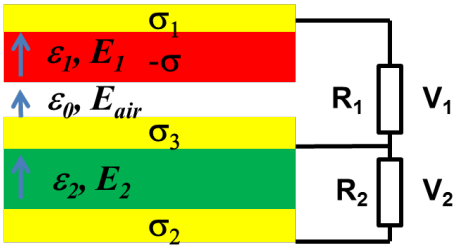

(i) Electric fields

Figure 5. Working mechanism of the HG. a) Schematic diagram of the device, b) the dependency curves of motion-time and force-time, c) inactive state. There is neither piezoelectric nor triboelectric output. d) The first stage (Δt_1, stage from t_1 to t_2). The upper cover and moving plate moves up with the displacement of the active layers η to zero. The piezoelectric potentials are generated. e) The second stage (Δt_2, stage from t_2 to t_3). The upper cover and moving plate moves up with the increase of x to x_{max}. Electrons are driven back from electrode 1 to electrode 2. f) The third stage (Δt_3, stage from t_3 to t_4). The moving plate moves up and down. There is neither piezoelectric nor triboelectric output generated. g) The fourth stage (Δt_4, stage from t_4 to t_5). The gap distance x begins to decrease from x_{max} to zero. Electrons are driven from electrode 2 to electrode 1. h) The fifth stage (Δt_5, stage from t_5 to t_6). The surface of the triboelectric layer begins to contact with electrode 2 and the piezoelectric layer is pressed with deformation. Piezoelectric potentials are generated and distributed on the two electrodes of piezoelectric unit. (i) schematic diagram of electric fields.

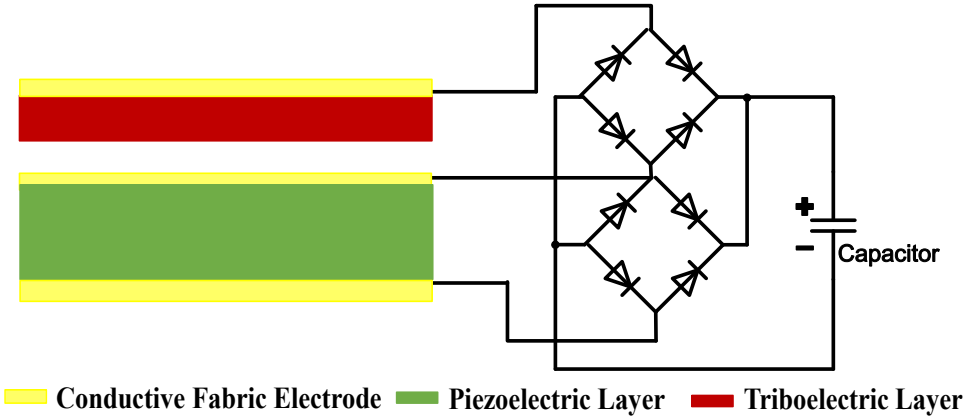

Figure 6. Schematic of the HG with a capacitor load in parallel connection